Analogues for the Molybdenum Center of Sulfite Oxidase: Oxomolybdenum(V) Complexes with Three Thiolate Sulfur Donor Atoms

M. L. Mader, Michael D. Carducci, and John H. Enemark*

Department of Chemistry, University of Arizona, Tucson, Arizona 85721-0041

Received June 30, 1999

cis,trans-(L-N_2S_2)Mo^VO(SR) [L-$N_2S_2H_2$ = *N,N′*-dimethyl-*N,N′*-bis(mercaptophenyl)ethylenediamine; R = CH_2-Ph, CH_2CH_3, and *p*-C_6H_4−Y (Y = CF_3, Cl, Br, F, H, CH_3, CH_2CH_3, and OCH_3)] are the first structurally characterized mononuclear Mo compounds with three thiolate donors, as occurs at the Mo active site in sulfite oxidase. X-ray crystal structures of the *cis,trans*-(L-N_2S_2)Mo^VO(SR) compounds, where R = CH_2Ph, CH_2CH_3, *p*-C_6H_4−OCH_3, and *p*-C_6H_4−CF_3, show a similar coordination geometry about the Mo atom with all three sulfur thiolate donors in the equatorial plane. This coordination geometry places two adjacent S p_π orbitals parallel to the Mo═O bond, analogous to the orientation in the ene-dithiolate ligand in sulfite oxidase; the third S p_π orbital lies in the equatorial plane. Charge-transfer transitions from the S p to the Mo d orbitals occur at approximately 28 000 cm^{-1} (ϵ: 4400−6900 L mol^{-1} cm^{-1}) and 15 500 cm^{-1} (ϵ: 3200−4900 L mol^{-1} cm^{-1}). The EPR parameters are nearly identical for all the *cis,trans*-(L-N_2S_2)Mo^VO(SR) compounds ($g_1 \sim 2.022$, $g_2 \sim 1.963$, $g_3 \sim 1.956$, $A_1 \sim 58.4 \times 10^{-4}$ cm^{-1}, $A_2 \sim 23.7 \times 10^{-4}$ cm^{-1}, $A_3 \sim 22.3 \times 10^{-4}$ cm^{-1}) and are typical of an oxo-Mo(V) center coordinated by multiple thiolate donors. The **g** and **A** tensors are related by a 24° rotation about the coincident g_2 and A_2 tensor elements, reflecting the approximate C_s coordination symmetry. These EPR parameters more closely mimic those of the low pH form of sulfite oxidase and the "very rapid" species of xanthine oxidase than previous model compounds with two or four thiolate donors. The *cis,trans*-(L-N_2S_2)Mo^VO(SR) compounds undergo a quasi-reversible, one-electron reduction and an irreversible oxidation that show a linear dependence upon the Hammett parameter, σ_p, of the Y group. The *cis,trans*-(L-N_2S_2)Mo^VO(SR) compounds provide a well-defined platform for the systematic investigation of the electronic structures of the Mo^VOS_3 centers and their implications for molybdoenzymes.

Introduction

Molybdenum is associated with more than 30 enzymes that catalyze two-electron oxidation−reduction reactions that are of crucial importance in the metabolism of C, N, and S by all forms of life.[1] These enzymes have been classified into three families,[1] primarily on the basis of the coordination about the molybdenum atom as revealed by X-ray absorption spectroscopy (XAS)[2−6] and recent X-ray crystal structures.[7−14] Sulfite oxidase has been shown to contain a $[Mo^{VI}O_2]^{2+}$ core in its fully oxidized state by XAS studies.[15] During enzymatic turnover, the molybdenum center is proposed to shuttle through the $Mo^{IV}/Mo^V/Mo^{VI}$ oxidation states.[16] The 1.9 Å crystal structure of chicken liver sulfite oxidase (SO) shows a novel five-coordinate, square pyramidal Mo center (Figure 1). A terminal oxo group was found in the axial position along with three thiolate S atoms in equatorial positions, one from a cysteine side chain and the two from the ene-dithiolate (dithiolene) of the pyranopterin[17,18] (molybdopterin)[19,20] found in all molybdoenzymes. The fourth equatorial position is occupied by an O atom that appears to be an OH or a H_2O ligand. This result suggests that the Mo center may have become reduced to Mo(V) or Mo(IV) by synchrotron radiation.[15] The sixth coordination site, trans to the apical oxo ligand, is blocked by the protein backbone and is not accessible

* Author to whom all correspondence should be addressed.

(1) Hille, R. *Chem. Rev.* **1996**, *96*, 2757−2816.
(2) Hille, R.; George, G. N.; Eidsness, M. K.; Cramer, S. P. *Inorg. Chem.* **1989**, *28*, 4018−4022.
(3) George, G. N.; Prince, R. C.; Mukund, S.; Adams, M. W. W. *J. Am. Chem. Soc.* **1992**, *114*, 3521−3523.
(4) George, G. N.; Garrett, R. M.; Prince, R. C.; Rajagopalan, K. V. *J. Am. Chem. Soc.* **1996**, *118*, 8588−8592.
(5) Baugh, P. E.; Garner, C. D.; Charnock, J. M.; Collison, D.; Davies, E. S.; McAlpine, A. S.; Bailey, S.; Lane, I.; Hanson, G. R.; McEwan, A. G. *JBIC, J. Biol. Inorg. Chem.* **1997**, *2*, 634−643.
(6) George, G. N.; Hilton, J.; Temple, C.; Prince, R. C.; Rajagopalan, K. V. *J. Am. Chem. Soc.* **1999**, *121*, 1256−1266.
(7) Kisker, C.; Schindelin, H.; Rees, D. C. *Annu. Rev. Biochem.* **1997**, *66*, 233−267.
(8) McAlpine, A. S.; McEwan, A. G.; Shaw, A. L.; Bailey, S. J. *JBIC, J. Biol. Inorg. Chem.* **1997**, *2*, 690−701.
(9) Boyington, J. C.; Gladyshev, V. N.; Khangulov, S. V.; Stadtman, T. C.; Sun, P. D. *Science* **1997**, *275*, 1305−1308.
(10) McAlpine, A. S.; McEwan, A. G.; Bailey, S. *J. Mol. Biol.* **1998**, *275*, 613−623.
(11) Kisker, C.; Schindelin, H.; Pacheco, A.; Wehbi, W. A.; Garrett, R. M.; Rajagopalan, K. V.; Enemark, J. H.; Rees, D. C. *Cell* **1997**, *91*, 973−983.
(12) Czjzek, M.; Dos Santos, J.-P.; Pommier, J.; Giordano, G.; Méjean, V.; Haser, R. *J. Mol. Biol.* **1998**, *284*, 435−447.
(13) Dias, J. M.; Than, M. E.; Humm, A.; Huber, R.; Bourenkov, G. P.; Bartunik, H. D.; Bursakov, S.; Calvete, J.; Caldeira, J.; Carneiro, C.; Moura, J. J. G.; Moura, I.; Romão, M. J. *Structure* **1999**, *7*, 65−79.
(14) Dobbek, H.; Gremer, L.; Meyer, O.; Huber, R. *Proc. Natl. Acad. Sci. U.S.A.* **1999**, *96*, 8884−8889.
(15) George, G. N.; Pickering, I. J.; Kisker, C. *Inorg. Chem.* **1999**, *38*, 2539−2540.
(16) Rajagopalan, K. *Molybdenum and Molybdenum Containing Enzymes*; M. Coughlan, Ed.; Pergamon: Oxford, 1980; pp 241−272.
(17) Hille, R. *JBIC, J. Biol. Inorg. Chem.* **1997**, *2*, 804−809.
(18) Fischer, B.; Enemark, J. H.; Basu, P. *J. Inorg. Biochem.* **1998**, *72*, 13−21.
(19) Rajagopalan, K. V. *Adv. Enzymol. Relat. Areas Mol. Biol.* **1991**, *64*, 215−290.
(20) Rajagopalan, K. V.; Johnson, J. L. *J. Biol. Chem.* **1992**, *267*, 10199−10202.

10.1021/ic990768o CCC: $19.00
Published on Web 01/21/2000

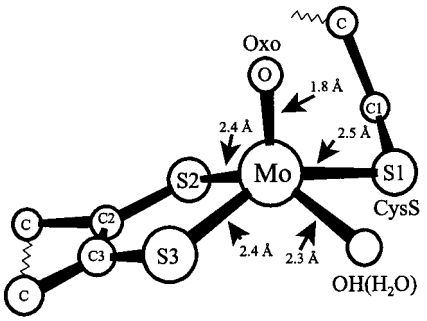

Figure 1. Mo center of chicken liver sulfite oxidase.[11] Bond angles (deg): S(1)−Mo−S(2), 93; S(1)−Mo−S(3), 147; S(2)−Mo−S(3), 84; Oxo−Mo−S(1)−C(1), 88; Oxo−Mo−S(2)−C(2), 98; Oxo−Mo−S(3)−C(3), 117.

to substrate or other ligands. It has been postulated that the "very rapid" signal exhibited by xanthine oxidase results from a $MoOS_3$ coordination site containing two S atoms from the molybdopterin and one S atom from a terminal sulfido ligand.[2,21−26]

There are no structurally characterized mononuclear oxo-Mo compounds with three S donor atoms, although several $Mo^{V}OS_3$ species have been proposed from solution EPR studies.[23,24,27−30] Our initial approach to the synthesis of analogues of the Mo(V) center of SO adopts the L-$N_2S_2H_2$[31] ligand, previously used by Spence, Wedd and co-workers[28,30] to mimic the Mo coordination environment in xanthine oxidase. This ligand forms isomeric mononuclear six-coordinate (L-N_2S_2)$Mo^{V}OX$ (X = Cl, NCS, Br, OEt, $OSiMe_3$, OPh, and SPh) compounds in which X and the two S atoms of L-N_2S_2 are in the equatorial plane.[30] Thus, for X = SR, either isomer should place three S atoms in the equatorial plane, as occurs for the Mo center of the sulfite oxidase and xanthine oxidase families. The sixth coordination site trans to the oxo group is occupied by one of the N atoms of the L-N_2S_2 ligand, thereby precluding interaction with other groups. Herein are presented the synthesis and characterization of the *cis*,*trans*-(L-N_2S_2)$Mo^{V}O$(SR) compounds, R = CH_2Ph, CH_2CH_3, and *p*-C_6H_4−Y (where Y = CF_3, Cl, Br, F, H, CH_3, CH_2CH_3, and OCH_3), which provide insight into the electronic structure and magnetic properties of $Mo^{V}OS_3$ sites.

Experimental Section

Materials. Unless otherwise stated, all operations were performed under an inert atmosphere with dried and deaerated solvents using Schlenk techniques. Microanalyses were performed by Desert Analytics, Tucson, Arizona.

N,*N*′-dimethyl-*N*,*N*′-bis(2-mercaptophenyl)ethylenediamine (L-$N_2S_2H_2$) was synthesized as previously reported.[28,30] The total yield of L-$N_2S_2H_2$ from 2-hydroxybenzothiazole (Aldrich) was improved from 30% to 40% by altering the amount of $ZnCl_2$ used in the reductive ammination reaction (from 0.37 mol $ZnCl_2$/1.0 mol *N*-methyl-2,*S*-benzylaniline to 0.93 mol $ZnCl_2$/1.0 mol *N*-methyl-2,*S*-benzylaniline). *cis*,*cis*-(L-N_2S_2)$Mo^{V}OCl$ was also prepared as previously reported.[28,30] All *cis*,*trans*-(L-N_2S_2)$Mo^{V}O$(SR) compounds, R = CH_2CH_3 and *p*-C_6H_4−Y (where Y = CF_3, Cl, Br, F, H, CH_3, CH_2CH_3, and OCH_3) were prepared by a manner analogous to that for *cis*,*trans*-(L-N_2S_2)$Mo^{V}O(SCH_2Ph)$.

***cis*,*trans*-(L-N_2S_2)$Mo^{V}O(SCH_2Ph)$ (1).** To a solution of *cis*,*cis*-(L-N_2S_2)$Mo^{V}OCl$ (0.202 g, 0.127 mmol) in THF (25.0 mL), $PhCH_2SH$ (1.4356 g; 11.559 mmol) and Et_3N (3 mL; 20 mmol) in EtOH (10.0 mL) were added. The solution immediately turned royal blue and was stirred for 24 h. The solvent was removed in vacuo. The residue was extracted with a minimal amount of CH_2Cl_2, and the solution was applied to a silica gel column (70−230 mesh, 15.0 cm × 2.5 cm diameter) and eluted with CH_2Cl_2. The first blue band was collected, concentrated in vacuo, and layered with hexanes. Dark-blue crystalline platelets were collected and dried. Yield: 0.1091 g (45%); EI-MS: *m*/*z* 539 (M^+). ν(Mo═O): 934 cm^{-1}. Anal. Calcd for $C_{23}H_{25}MoN_2OS_3$: C, 51.39; H, 4.69; N, 5.21; S, 17.89. Found: C, 51.30; H, 4.88; N, 5.09; S, 18.10.

***cis*,*trans*-(L-N_2S_2)$Mo^{V}O(SCH_2CH_3)$ (2).** Lustrous blue rectangular crystals were produced in a 54% yield. ESI-MS: *m*/*z* 477 (M^+). ν(Mo═O): 936 cm^{-1}. Anal. Calcd for $C_{18}H_{23}MoN_2OS_3$: C, 45.47; H, 4.88; N, 5.89; S, 20.23. Found: C, 45.46; H, 4.91; N, 5.69; S, 20.58.

***cis*,*trans*-(L-N_2S_2)$Mo^{V}O$(*p*-$SC_6H_4OCH_3$) (3).** Dark blue lustrous crystals were prepared in a 24% yield. EI-MS: *m*/*z* 555 (M^+); M^+ extremely weak. ν(Mo═O): 928 cm^{-1}. Anal. Calcd for $C_{23}H_{25}MoN_2O_2S_3$: C, 49.90; H, 4.55; N, 5.06; S, 17.37. Found: C, 49.51; H, 4.46; N, 4.90; S, 17.26.

***cis*,*trans*-(L-N_2S_2)$Mo^{V}O$(*p*-$SC_6H_4CH_2CH_3$) (4).** Dark blue-green platelets were prepared in a 56% yield. EI-MS: *m*/*z* 552 (M^+). ν(Mo═O): 934 cm^{-1}. Anal. Calcd for $C_{24}H_{27}MoN_2OS_3$: C, 52.26; H, 4.93; N, 5.08; S, 17.44. Found: C, 51.96; H, 4.81; N, 4.93; S, 17.17.

***cis*,*trans*-(L-N_2S_2)$Mo^{V}O$(*p*-$SC_6H_4CH_3$) (5).** A dark-green shiny powder was prepared in a 76% yield. EI-MS: *m*/*z* 539 (M^+). ν(Mo═O): 932 cm^{-1}. Anal. Calcd for $C_{23}H_{25}MoN_2OS_3$: C, 51.39; H, 4.69; N, 5.21; S, 17.89. Found: C, 51.29; H, 4.71; N, 5.06; S, 17.62.

***cis*,*trans*-(L-N_2S_2)$Mo^{V}O(SC_6H_5)$ (6).** A dark-green, powder was prepared in an 80% yield with slight modifications to the previously reported synthesis.[30] EI-MS: *m*/*z* 525 (M^+). ν(Mo═O): 927 cm^{-1}.

***cis*,*trans*-(L-N_2S_2)$Mo^{V}O$(*p*-SC_6H_4F) (7).** A dark-green, shiny powder was prepared in a 70% yield. EI-MS: *m*/*z* 543 (M^+). ν(Mo═O): 929 cm^{-1}. Anal. Calcd for $C_{22}H_{22}MoFN_2OS_3$: C, 48.79; H, 4.09; N, 5.17; S, 17.76. Found: C, 48.51; H, 4.32; N, 4.92; S, 17.41.

***cis*,*trans*-(L-N_2S_2)$Mo^{V}O$(*p*-SC_6H_4Br) (8).** Dark forest-green needles were produced in a 63% yield. ν(Mo═O): 929 cm^{-1}. Anal. Calcd for $C_{22}H_{22}MoBrN_2OS_3$: C, 43.86; H, 3.68; N, 4.65; S, 15.96. Found: C, 43.84; H, 3.57; N, 4.39; S, 16.12.

***cis*,*trans*-(L-N_2S_2)$Mo^{V}O$(*p*-SC_6H_4Cl) (9).** Dark forest-green needles were synthesized in a 67% yield. EI-MS: *m*/*z* 559 (M^+). ν(Mo═O): 929 cm^{-1}. Anal. Calcd for $C_{22}H_{22}MoClN_2OS_3$: C, 47.35; H, 3.97; N, 5.02; S, 17.23. Found: C, 46.61; H, 3.77; N, 4.67; S, 17.19.

***cis*,*trans*-(L-N_2S_2)$Mo^{V}O$(*p*-$SC_6H_4CF_3$) (10).** Dark blue-green rectangular crystals were prepared in a 56% yield. EI-MS: *m*/*z* 593 (M^+). ν(Mo═O): 943 cm^{-1}. Anal. Calcd for $C_{23}H_{22}MoF_3N_2OS_3$: C, 46.70; H, 3.75; N, 4.74; S, 16.26. Found: C, 47.26; H, 3.78; N, 4.55; S, 15.94.

Crystal Structure Determinations. Single crystals of *cis*,*trans*-(L-N_2S_2)$Mo^{V}O(SCH_2Ph)$ (**1**), *cis*,*trans*-(L-N_2S_2)$Mo^{V}O(SCH_2CH_3)$ (**2**), and *cis*,*trans*-(L-N_2S_2)$Mo^{V}O$(*p*-SC_6H_4−OCH_3) (**3**) complexes were grown by diffusion of hexanes into a CH_2Cl_2 solution of the complex. Single crystals of *cis*,*trans*-(L-N_2S_2)$Mo^{V}O$(*p*-SC_6H_4−CF_3) (**10**) were grown by diffusion of pentane into a THF solution of the complex.

Selected crystallographic data are given in Table 1. Further data are given in the Supporting Information. For **1** and **10**, the intensity data were collected on a Bruker AXS single-crystal diffractometer with a SMART 1000 CCD detector. For **2** and **3**, intensity data were collected on an Enraf-Nonius CAD-4MachS single-crystal diffractometer. Both diffractometers use Mo Kα radiation with a graphite crystal monochromator. The intensity data were corrected for Lorentz and polariza-

(21) Cramer, S. P.; Hille, R. *J. Am. Chem. Soc.* **1985**, *107*, 8164−8169.
(22) George, G. N.; Bray, R. C. *Biochemistry* **1988**, *27*, 3603−3609.
(23) Wilson, G. L.; Greenwood, R. J.; Pilbrow, J. R.; Spence, J. T.; Wedd, A. G. *J. Am. Chem. Soc.* **1991**, *113*, 6803−6812.
(24) Greenwood, R. J.; Wilson, G. L.; Pilbrow, J. R.; Wedd, A. G. *J. Am. Chem. Soc.* **1993**, *115*, 5385−5392.
(25) Romão, M. J.; Archer, M.; Moura, J. J. G.; LeGall, J.; Engh, R.; Schneider, M.; Hof, P.; Huber, R. *Science* **1995**, *270*, 1170−11776.
(26) Huber, R.; Hof, P.; Duarter, R. O.; Moura, J. J. G.; Moura, I.; Liu, M.; LeGall, J.; Hille, R.; Archer, M.; Romão, M. *Proc. Natl. Acad. Sci. U.S.A.* **1996**, *93*, 8846−8851.
(27) Guiles, R. D. M.S. Thesis, San Francisco State University, San Francisco, CA, 1983.
(28) Dowerah, D.; Spence, J. T.; Singh, R.; Wedd, A. G.; Wilson, G. L.; Farchione, F.; Enemark, J. H.; Kristofski, J.; Bruck, M. *J. Am. Chem. Soc.* **1987**, *109*, 5655−5665.
(29) Hahn, R.; Küsthardt, U.; Scherer, W. *Inorg. Chim. Acta* **1993**, *210*, 177−182.
(30) Barnard, K. R.; Bruck, M.; Huber, S.; Grittini, C.; Enemark, J. H., Gable, R. W.; Wedd, A. G. *Inorg. Chem.* **1997**, *36*, 637−649.

Table 1. Crystallographic Data

	cis,trans-(L-N_2S_2)$Mo^{V}O(SCH_2Ph)$ (**1**)	*cis,trans*-(L-N_2S_2)$Mo^{V}O(SCH_2CH_3)$ (**2**)	*cis,trans*-(L-N_2S_2)$Mo^{V}O(p\text{-}SC_6H_4OCH_3)$ (**3**)	*cis,trans*-(L-N_2S_2)$Mo^{V}O(p\text{-}SC_6H_4CF_3)$ (**10**)
formula	$C_{23}H_{25}MoN_2OS_3$	$C_{23}H_{25}MoN_2OS_3$	$C_{23}H_{25}MoN_2O_2S_3$	$C_{23}H_{22}F_3MoN_2O_2S_3$
color, shape	blue, plate	blue, rectangular	green, rectangular	blue-green, rectangular
dimensions (mm)	0.46 × 0.36 × 0.04	0.43 × 0.29 × 0.17	0.42 × 0.17 × 0.13	0.22 × 0.09 × 0.09
fw, g mol^{-1}	537.57	475.51	553.58	591.55
crystal system	monoclinic	orthorhombic	monoclinic	orthorhombic
a, Å	9.4552(3)	11.554(1)	17.949(2)	8.1879(8)
b, Å	11.8425(4)	14.263(1)	7.6666(8)	15.761(2)
c, Å	11.1758(4)	24.454(2)	17.973(5)	18.299(2)
β, deg	112.361(1)		107.93(2)	
V, Å^3	1157.29(6)	4029.9(5)	2353.1(7)	2361.5(4)
Z	2	8	4	4
space group	$P2_1$ (#4)	*P*bca (#61)	$P2_1/n$ (#14)	$P2_12_12_1$ (#19)
ρ, g cm^{-1}	1.543	1.567	1.562	1.664
μ, cm^{-1}	8.54	9.69	8.45	8.63
$T_{min} - T_{max}$	0.688−0.983	0.926−1.000	0.933−0.999	0.713−0.981
scan method	ω scans	$\omega/2\theta$	$\omega/2\theta$	ω scans
$2\theta_{max}$, deg	56.6	49.9	49.9	56.6
no. of data	7976	3997	4627	20810
no. of data, unique	2972	3997	4481	3323
no. of data, refined	2678 ($I > 2\sigma(I)$)	2302 ($I > 3\sigma(I)$)	2588 ($I > 3\sigma(I)$)	2682 ($I > 2\sigma(I)$)
no. of parameters	270	101	280	298
max peak height, e·Å^{-3}	0.56	0.95	1.45	0.45
R^a	0.030	0.042	0.049	0.030
$R_w{}^b$	0.032	0.038	0.047	0.025
GOF	1.18	1.96	1.88	0.62

[a] $R = \sum||F_o| - |F_c||/\sum|F_o|$. [b] $R_w = \sum w||F_o| - |F_c||^2/\sum w|F_o|^2$.

tion effects. Structures were solved by direct methods using SIR-92,[32] and least-squares refinement (based on F) was performed using teXsan.[33]

***cis,trans*-(L-N_2S_2)$Mo^{V}O(SCH_2Ph)$ (1) and *cis,trans*-(L-N_2S_2)-$Mo^{V}O(p\text{-}SC_6H_4CF_3)$ (10).** The data were integrated using the SAINT program,[34] and an empirical absorption correction using SADABS[35] was applied. The final unit cell was determined from 7976 reflections for **1** and 7611 reflections for **10**, derived from the full data set. All hydrogen atoms were constrained during refinement using the riding model. The absolute stereochemistry was determined by refinement of the Flack parameter.[36]

***cis,trans*-(L-N_2S_2)$Mo^{V}O(SCH_2CH_3)$ (2) and *cis,trans*-(L-N_2S_2)-$Mo^{V}O(p\text{-}SC_6H_4OCH_3)$ (3).** The unit cell parameters were determined from least-squares refinement of the setting angles for 25 reflections with 9.87° < 2θ < 17.38° for **2** and with 8.06° < 2θ < 13.29° for **3**. Two reflections were monitored every 60 min during data collection and showed no intensity variation. An absorption correction was applied using psi-scans. All hydrogen atoms were constrained during refinement using the riding model.

Physical Techniques. IR spectra were recorded on a Nicolet Avatar ESP 360 FT-IR spectrometer in a matrix of KBr. Electronic spectra were recorded on an Olis modified Cary-14 spectrophotometer from 33 300 to 12 500 cm^{-1}. The near-infrared (NIR) region of toluene solutions of **1**, **3**, and **10** (12 500−6600 cm^{-1}) were acquired using a dual-beam Hitachi U-3501 UV−vis NIR spectrophotometer. The NIR electronic spectra were collected at 2.0-nm resolution in a dual-beam configuration, and the instrument was calibrated with reference to known lines of a mercury lamp and a piece of glass doped with 6% neodymium. The NIR electronic spectra were collected in 1-cm path length Helma quartz cells, equipped with a Teflon stopper. An Analytica electrospray source was used to ionize **1** in acetonitrile. The mass spectrum was recorded on a JEOL HIX 110A high-resolution sector instrument. Electron impact mass spectra (EI-MS) of **2**−**10** were performed on a Hewlett-Packard 5988A GC/MS system.

EPR spectra at X-band frequency of solution (298 K) and frozen glasses (77 K) were recorded on a Bruker ESP 300 spectrometer. The conditions, solvents, and glassing agents are given in the Supporting Information (Table S34). EPR spectra of **1** at S-band and Q-band frequencies were recorded in a mixture of toluene and CH_2Cl_2. The S-band frozen spectrum was recorded at 116 K, and the Q-band frozen spectrum was recorded at 110 K. The spectra were simulated using the program QPOW.[37]

Cyclic voltammetry was performed in acetonitrile solutions (3 × 10^{-4} − 1 × 10^{-3} M complex) over a potential range of 1.1 to −1.1 V vs Ag/Ag^+ with 0.09 M tetra-*n*-butylammonium tetrafluoroborate [*n*-Bu_4N][BF_4] (Alfa) as the supporting electrolyte. The acetonitrile (EM Science, OmniSolv, distilled) was triply distilled.[38] Background scans of deoxygenated acetonitrile with ∼0.09 M [*n*-Bu_4N][BF_4] exhibited no impurities or solvent degradation in the potential window observed. The electrochemical cell consisted of a platinum disk (1.6 mm) working electrode (Bioanalytical Systems, BAS), platinum wire counter electrode (BAS), and KCl saturated Ag/Ag^+ reference electrode (BAS). The platinum disk electrode was polished using alumina (BAS). Prior to each experiment, the electrode was cleaned by performing bulk electrolysis at 900 mV and −900 mV in 6 M HNO_3. All scans were performed with a BAS CV-50W potentiostat under the control of BAS software. Ferrocene was used as an internal standard, and all potentials were referenced to the Fc/Fc^+ couple.

Results and Discussion

Structural Characterization. X-ray crystal structure determinations for **1**−**3** and **10** show that the compounds adopt

(31) Abbreviations: L-$N_2S_2H_2$: *N*,*N*′-dimethyl-*N*,*N*′-bis(mercaptophenyl)-ethylenediamine; tp*: hydrotris(3,5-dimethyl-1-pyrazolyl)borate; bdt: 1,2-benzenedithiolate.

(32) Altomare, A.; Cascarano, M.; Giacovazzo, C.; Guagliardi, A. *J. Appl. Crystallogr.* **1993**, *26*, 343.
(33) *teXsan*: *Single-Crystal Structure Analysis Software*, version 1.8; Molecular Structure Corporation: The Woodlands, TX, 1992, 1997.
(34) *SAINT* version 5.01, *Software for the CCD Detector System*. Brucker Analytical X-ray System: Madison, WI, 1998.
(35) *SADABS*. *Program for Absorption Corrections Using Seimens CCD Based in the Method of Robert Blessing*. Blessing, R. H. *Acta Crystallogr.* **1995**, *A51*, 33−38.
(36) Flack, H. *Acta Crystallogr.* **1983**, *A39*, 876−881.
(37) Nigles, M. J. Ph.D Dissertation, Univerity of Illinois, Urbana, IL, 1979. Belford, R. L.; Nigles, M. J. EPR Symposium, 21st Rocky Mountain Conference: Denver, CO, August 1979. Maurice, A. M. Ph.D Dissertation, University of Illinois, Urbana, IL, 1980.
(38) Perrin, D.; Armarego, W.; Perrin, D. *Purification of Laboratory Chemicals*, 2nd ed.; Pergamon Press: New York, 1980.

Table 2. Selected Bond Distances, Bond Angles, and Torsional Angles

cis,trans-(L-N_2S_2)$Mo^{V}O(SCH_2Ph)$ (**1**)	*cis*,trans-(L-N_2S_2)$Mo^{V}O(SCH_2CH_3)$ (**2**)	*cis*,trans-(L-N_2S_2)$Mo^{V}O$(*p*-$SC_6H_4OCH_3$) (**3**)	*cis*,trans-(L-N_2S_2)$Mo^{V}O$(*p*-$SC_6H_4CF_3$) (**10**)
		Bond Distances (Å)	
Mo1−S2: 2.356(1)	Mo1−S2: 2.338(2)	Mo1−S2: 2.365(2)	Mo1−S2: 2.389(2)
Mo1−S3: 2.388(1)	Mo1−S3: 2.378(2)	Mo1−S3: 2.378(2)	Mo1−S3: 2.379(2)
Mo1−S4: 2.402(1)	Mo1−S4: 2.418(2)	Mo1−S4: 2.409(2)	Mo1−S4: 2.393(2)
Mo1−O5: 1.683(3)	Mo1−O5: 1.667(4)	Mo1−O5: 1.693(5)	Mo1−O5: 1.676(3)
Mo1−N6: 2.312(3)	Mo1−N6: 2.320(4)	Mo1−N6: 2.311(5)	Mo1−N6: 2.313(4)
Mo1−N7: 2.517(3)	Mo1−N7: 2.508(4)	Mo1−N7: 2.512(6)	Mo1−N7: 2.538(4)
S2−C8: 1.828(4)	S2−C8: 1.886(8)	S2−C9: 1.787(7)	S2−C8: 1.781(5)
S3−C15: 1.770(4)	S3−C10: 1.759(5)	S3−C16: 1.762(7)	S3−C15: 1.772(5)
S4−C23:1.754(4)	S4−C18:1.736(6)	S4−C24:1.747(7)	S4−C23: 1.765(5)
		Bond Angles (deg)	
S2−Mo1−S3: 83.90(4)	S2−Mo1−S3: 91.55(6)	S2−Mo1−S3: 91.17(7)	S2−Mo1−S3: 94.76(5)
S2−Mo1−S4: 96.66(4)	S2−Mo1−S4: 88.39(6)	S2−Mo1−S4: 86.60(7)	S2−Mo1−S4: 83.69(5)
S2−Mo1−O5: 104.9(1)	S2−Mo1−O5: 105.9(2)	S2−Mo1−O5: 104.4(2)	S2−Mo1−O5: 104.9(1)
S3−Mo1−S4: 162.56(4)	S3−Mo1−S4: 162.68(6)	S3−Mo1−S4: 161.01(8)	S3−Mo1−S4: 160.89(6)
S3−Mo1−O5: 104.5(1)	S3−Mo1−O5: 104.5(2)	S3−Mo1−O5: 104.4(2)	S3−Mo1−O5: 104.0(1)
S4−Mo1−O5: 92.2(1)	S4−Mo1−O5: 92.2(1)	S4−Mo1−O5: 94.4(2)	S4−Mo1−O5: 94.8(1)
Mo1−S2−C8: 111.8(2)	Mo1−S2−C8: 114.0(2)	Mo1−S2−C9: 110.9(2)	Mo1−S2−C8: 113.9(2)
Mo1−S3−C15: 99.6(1)	Mo1−S3−C10: 101.4(2)	Mo1−S3−C16: 99.7(2)	Mo1−S3−C15: 101.1(2)
Mo1−S4−C23: 106.9(1)	Mo1−S4−C18: 106.5(2)	Mo1−S4−C24: 107.7(2)	Mo1−S4−C23: 106.7(2)
O5−Mo1−N6: 91.4(1)	O5−Mo1−N6: 90.8(2)	O5−Mo1−N6: 90.1(2)	O5−Mo1−N6: 93.5(2)
O5−Mo1−N6: 162.0(1)	O5−Mo1−N6: 161.1(2)	O5−Mo1−N6: 161.0(2)	O5−Mo1−N7: 164.9(2)
		Torsional Angles (deg)	
O5−Mo1−S2−C8: 96.9(3)	O5−Mo1−S2−C8: −91.4(4)	O5−Mo1−S2−C9: −81.9(3)	O5−Mo1−S2−C8: −89.0(2)
O5−Mo1−S3−C15: −71.0(2)	O5−Mo1−S3−C10: −77.4(3)	O5−Mo1−S3−C16: −69.6(3)	O5−Mo1−S3−C15: −80.6(3)
O5−Mo1−S4−C23: 169.1(2)	O5−Mo1−S4−C18: 173.5(2)	O5−Mo1−S4−C24: 159.7(3)	O5−Mo1−S4−C23: 177.9(2)

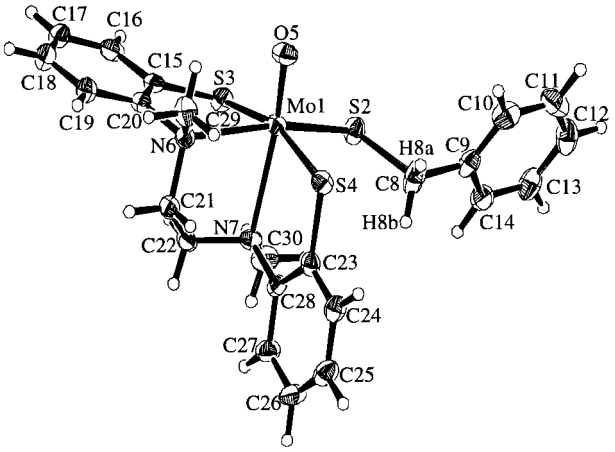

Figure 2. ORTEP of *cis,trans*-(L-N_2S_2)$Mo^{V}O(SCH_2Ph)$ (**1**).

cis,trans geometry,[30] as depicted in Figures 2 (Compound **1**) and S1−S3, with all three S atoms in the equatorial plane perpendicular to the Mo═O bond. Compounds **1**−**3** and **10** possess three chiral centers, namely at the molybdenum atom and the two nitrogen atoms. The relative configurations of the three stereocenters are the same for **1**−**3** and **10**. The structural parameters of **1**−**3** and **10** (Table 2) are similar to those of previously structurally characterized *cis,trans*-(L-N_2S_2)$Mo^{V}OX$ (X = NCS, Cl, $OSi(CH_3)_3$).[30] For **1**, the Mo atom is 0.350 Å out of the equatorial least-squares plane defined by S2−S3−S4−N6 and toward the oxo group. As a consequence, the Mo−N7 distance trans to the Mo═O bond is elongated by ∼0.2 Å relative to Mo−N6. The dihedral angle between the phenyl rings of the L-N_2S_2 ligand, a parameter used to characterize the stereochemistry of the coordinated ligand,[30] is 91.3° and is similar to the values found in other *cis,trans*-(L-N_2S_2)$Mo^{V}OX$ (X = NCS, Cl, $OSi(CH_3)_3$) compounds. The dihedral angles between the equatorial coordination plane (S2−S3−S4−N6) and the phenyl rings defined by C15−C20 and C23−C28 are 11.6° and 83.3°, respectively. Similar values for these structural parameters are found for **2**, **3**, and **10** (Supporting Information, Tables S9, S16, S24, and S32.) The major difference among structures **1**−**3** and **10** is the orientation of the SR group. In all four structures, the S2−C bond lies approximately in the equatorial plane. For **1**, the O5−Mo1−S2−C8 dihedral angle is 96.9(3)°, and the R group points toward S4 of the L-N_2S_2 ligand. However, for **2**, **3**, and **10** the corresponding angles are −91.4(4)° −81.9(3)°, and −89.0(2)°, respectively (Table 2), and the R group points toward S3 of the L-N_2S_2 ligand. Thus, the benzyl group of **1** is rotated by ∼180° about the Mo−S bond relative to the SR groups of **2**, **3**, and **10** (Figures 2 and S1 − S3). Space-filling models suggest that the steric barrier to rotation about the Mo−S2 bond should be small.

Chemically equivalent Mo−S distances are similar in **1**−**3** and **10** (Table 2) and comparable to the Mo−S distances found in chicken liver SO (Figure 1), (tp*)$Mo^{V}O(bdt)$,[31,39,40] (tp*)$Mo^{V}O(SPh)_2$,[41] $[Mo^{V}O(SPh)_4]^-$,[42] and $[Mo^{V}O(bdt)_2]^-$.[43] Although the *cis,trans*-(L-N_2S_2)$Mo^{V}O(SR)$ compounds do not possess an ene-dithiolate ligand, the orientation of the out-of-plane S p_π orbitals on S2 and S3 does mimic the orientation of the S p_π orbitals of an ene-dithiolate ligand (Figure 3). In the crystal structure of SO, the S p_π orbital of the coordinated S_{cys} ligand is also approximately parallel to the axial Mo═O bond. However, for **1**−**3** and **10**, the constraints of the L-N_2S_2 ligand place the S p_π orbital of S4 in the equatorial plane and perpendicular to the axial Mo═O bond. The structures of **1**−**3** and **10** are also related to the "very rapid" species of XO, which is proposed to have a third S donor atom from a sulfido ligand

(39) Dhawan, I. K.; Pacheco, A.; Enemark, J. H. *J. Am. Chem. Soc.* **1994**, *116*, 7911−7912.
(40) Dhawan, I. K.; Enemark, J. H. *Inorg. Chem.* **1996**, *35*, 4873−4882.
(41) Cleland, W. E., Jr.; Barnhart, K. M.; Yamanouchi, K.; Collison, D.; Mabbs, F. E.; Ortega, R. B.; Enemark, J. H. *Inorg. Chem.* **1987**, *26*, 1017−1025.
(42) Bradbury, J. R.; Mackay, M. F.; Wedd, A. G. *Aust. J. Chem.* **1978**, *31*, 2423−2430.
(43) Boyde, S.; Ellis, S. R.; Garner, C. D.; Clegg, W. *J. Chem. Soc., Dalton Trans.* **1986**, 1541−1543.

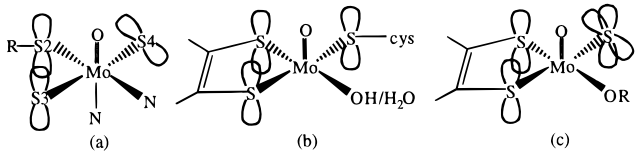

Figure 3. Coordination about the Mo centers of (a) (L-N_2S_2)$Mo^{V}O(SCH_2$-CH_3), (b) chicken liver sulfite oxidase, and (c) the proposed "very rapid" species of xanthine oxidase, depicting the relative orientation of the S p_π orbitals.

in the equatorial plane.[22−24] The sulfido ligand has two S p_π orbitals, one perpendicular and one parallel to the Mo═O group (Figure 3).

Spectroscopic Characterization. The similarity of the structures for the (L-N_2S_2)$Mo^{V}O$(SR) complexes means that differences in their spectroscopic properties should primarily reflect perturbations on the overall bonding interactions of the complexes due to the nature of the R group of the SR ligand. The electronic spectra (Figure S4) of the *cis*,*trans*-(L-N_2S_2)-$Mo^{V}O$(SR) complexes exhibit two broad bands near 15 500 cm^{-1} (ϵ: 3200−4900 L mol^{-1} cm^{-1}) and 28 000 cm^{-1} (4400−6900 L mol^{-1} cm^{-1}) (Table S33, Figure S4) with intensities characteristic of orbitally allowed LMCT [S p → Mo d] transitions. The intensity of the low-energy band is significantly greater[44] than previously observed for S p_π out-of-plane to d_{xy} transitions, and this band is most reasonably assigned to LMCT transitions from in-plane S p_π orbitals on S4 to the singly occupied orbital that is primarily Mo 4 d_{xy}.[44,45] The higher-energy envelope most likely involves transitions from out-of-plane S p_π orbitals to the Mo $d_{xz,yz}$ orbitals. The characteristic $d_{xy} \rightarrow d_{xz,yz}$ transitions of $[Mo{=}O]^{3+}$ centers that typically occur in the 12 000−19 000 cm^{-1} region[44] are presumed to be overlapped by the lower-energy LMCT band. The position of the lower energy band shifts by 1000 cm^{-1} to higher energy as the Y substituent becomes increasingly electron releasing. No additional bands are detected in the NIR region down to 6500 cm^{-1}.

The ligand field splitting of d orbitals in six-coordinate oxo-Mo(V) complexes is dominated by the short Mo═O bond, and the singly occupied d_{xy} orbital is the highest occupied molecular orbital (HOMO).[44] Sulfur ligands in the equatorial plane further modify the energy of the HOMO through electrostatic effects and by direct bonding/antibonding interactions with the d_{xy} orbital.[44,45] For the (L-N_2S_2)$Mo^{V}O$(SR) compounds, the primary in-plane bonding interaction with the d_{xy} orbital will involve the S p_π orbital of S4 of the L-N_2S_2 ligand (Figure 4). The filled S p_π orbitals of the SR ligand and of S3 from the L-N_2S_2 ligand are oriented approximately parallel to the Mo═O bond (Figure 3), and they will have little overlap with the Mo d_{xy} orbital.[44,45] All three S atoms also have in-plane S p orbitals that will primarily be involved in σ-bonding with $d_{x^2-y^2}$.[46]

The frozen solution S-, X-, and Q-band EPR spectra for **1** (Figure 5, Table 3) exhibit pseudoaxial **g** and **A**(^{95,97}Mo) tensors and monoclinic symmetry. This result is consistent with the approximate C_s coordination symmetry about the Mo atom, with the mirror plane containing the atoms Mo1, S2, O5, N6, and N7 (Figure 2). The effective C_s symmetry of **1** requires that the g_2 and A_2 tensor elements be coincident, approximately parallel

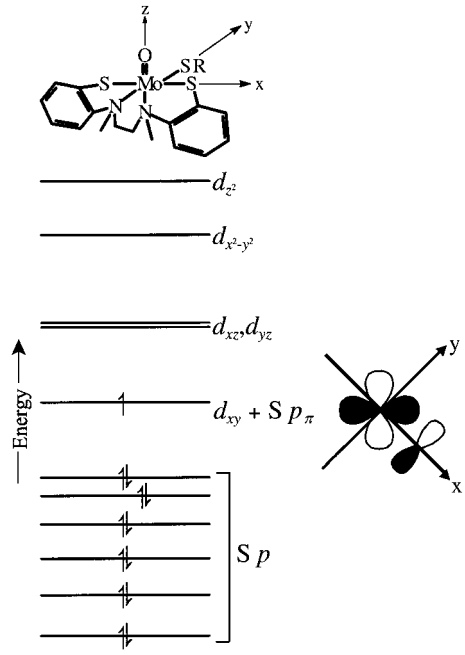

Figure 4. Energy-level diagram for the *cis*,*trans*-(L-N_2S_2)$Mo^{V}O$(SR) complexes depicting the HOMO, which is composed of the Mo d_{xy} and the in-plane S4 p_π orbitals.

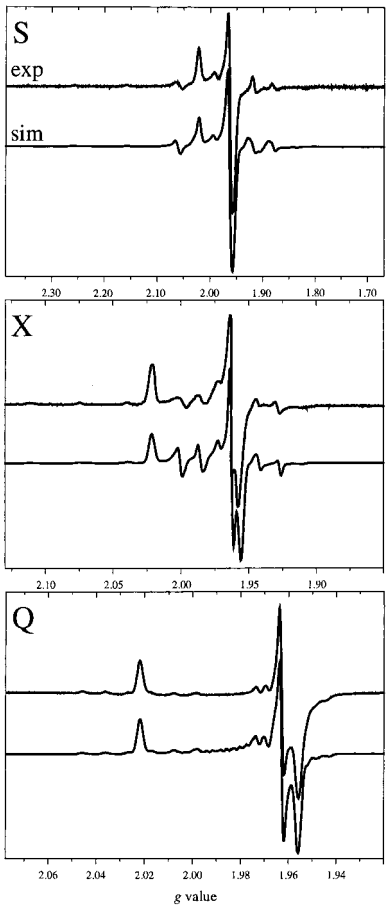

Figure 5. EPR spectra of *cis*,*trans*-(L-N_2S_2)$Mo^{V}O(SCH_2Ph)$ (**1**) at S-band, X-band, and Q-band. The simulated spectrum is shown below the experimental spectrum.

to the Mo−S4 bond, and contained within the equatorial coordination plane.[47−49] The largest A(^{95,97}Mo) value, A_1, is usually placed along the Mo═O bond because of the large influence that the Mo═O bond exerts on the ligand field.[47,50−52]

(44) Carducci, M. D.; Brown, C.; Solomon, E. I.; Enemark, J. H. *J. Am. Chem. Soc.* **1994**, *116*, 11856−11868.
(45) Inscore, F. E.; McNaughton, R.; Westcott, B. L.; Helton, M. E.; Jones, R.; Dhawan, I. K.; Enemark, J. H.; Kirk, M. L. *Inorg. Chem.* **1999**, *38*, 1401−1410.
(46) Gebhard, M. S.; Deaton, J. C.; Koch, S. A.; Millar, M.; Solomon, E. I. *J. Am. Chem. Soc.* **1990**, *112*, 2217−2231.

Table 3. EPR Data for Chicken Liver Sulfite Oxidase, Xanthine Oxidase, and Oxo-Molybdenum Complexes with Sulfur Donor Ligands

signal	g_1[a]	g_2	g_3	<g>	A_1[b]	A_2	A_3	<A>	α[c]	β	γ
sulfite oxidase (low-pH form)[h]	2.007	1.974	1.968	1.983	56.7	25.0	16.7	32.8	0	18	0
sulfite oxidase (high-pH form)[h]	1.990	1.966	1.954	1.970	54.4	21.0	11.3	28.9	0	14	22
xanthine oxidase (very rapid, xanthine)[i]	2.025	1.955	1.949	1.977	44.4	18.2	19.1	27.2	8	36	0
(tp*)$Mo^{V}O$(bdt)[h]	2.004	1.972	1.934	1.971	50.0	11.4	49.7	37.0	0	0	0
cis,trans-(L-N_2S_2)$Mo^{V}O(SCH_2Ph)$	2.022	1.963	1.956	1.980	58.4	23.7	22.3	34.8	0	24	0
$[MoO(SPh)_4]^{-}$[j]	2.017[d]	1.979[e]	1.979[e]	1.990	52.6[f]	23.0[g]	23.0[g]	31.5	0	0	0

[a] Error ± 0.001. [b] $A(^{95,97}Mo)$, × 10^{-4} cm^{-1}, errors ± 1 × 10^{-4} cm^{-1}. [c] Errors ± 2°. [d] $g_{||}$. [e] $g_{\perp}$. [f] $A_{||}$. [g] $A_{\perp}$. [h] Refs 39−40. [i] Ref 22. [j] Ref 42.

Table 4. Electrochemical Data for *cis,trans*-(L-N_2S_2)MoO(SR) Compounds

	(Mo^{V}/Mo^{IV})			(Mo^{V}/Mo^{VI})
compound	E_{mp}[a]	ΔE_p	$\lvert i_{pa}/i_{pc}\rvert$	E_{pa}[a]
cis,trans-(L-N_2S_2)MoO(SCH_2Ph) (**1**)	−1009	63	1.1	330
cis,trans-(L-N_2S_2)MoO(SCH_2CH_3) (**2**)	−1061	62	1.1	300−346
cis,trans-(L-N_2S_2)MoO(*p*-$SC_6H_4OCH_3$) (**3**)	−979	61	1.1	357
cis,trans-(L-N_2S_2)MoO(*p*-$SC_6H_4CH_2CH_3$) (**4**)	−964	59	1.1	401
cis,trans-(L-N_2S_2)MoO(*p*-$SC_6H_4CH_3$) (**5**)	−974	62	1.1	397
cis,trans-(L-N_2S_2)MoO(SC_6H_5) (**6**)	−949	74	1.4	419
cis,trans-(L-N_2S_2)MoO(*p*-SC_6H_4F) (**7**)	−935	62	1.1	441
cis,trans-(L-N_2S_2)MoO(*p*-SC_6H_4Br) (**8**)	−912	56	1.1	462
cis,trans-(L-N_2S_2)MoO(*p*-SC_6H_4Cl) (**9**)	−915	60	1.1	459
cis,trans-(L-N_2S_2)MoO(*p*-$SC_6H_4CF_3$) (**10**)	−887	64	1.1	491

[a] ΔE_{mp} ± 1 mV. All potentials are vs Fc/Fc^{+}.

Westmoreland and colleagues[53−55] have found that the largest g value, g_1, rotates away from the Mo═O vector and toward the equatorial plane as the covalency of the ligand bonds in the equatorial plane increases. Spectral simulation shows that the Euler angle, β, defined as rotation about the coincident g_2 and A_2 tensor elements, is 24° (Table 3). This rotation is interpreted as moving g_1 closer to the Mo−S equatorial plane. Single-crystal EPR studies will be required to determine if this postulated orientation of the **g** tensor relative to the molecular frame is correct.

The frozen solution X-band EPR spectral parameters (Table S34) for all 10 *cis,trans*-(L-N_2S_2)$Mo^{V}O$(SR) compounds are very similar, which indicates a common ground electronic state[56−58] for these compounds and supports the qualitative bonding picture proposed in Figure 4. The value of g_1 for **1**−**10** is larger than g_e, while g_2 and g_3 are smaller than g_e. Values of $g_1 > g_e$ are a common feature of compounds containing multiple sulfur donor ligands.[40,41,59,60] The large g values observed in such systems have previously been attributed to low-energy LMCT [S p→Mo d] charge-transfer bands, sulfur one-electron spin−orbit coupling,[61−63] and metal−ligand covalency.[53,54] Recent molecular orbital[53] and density functional[54] calculations on a series of oxo-Mo(V) complexes have shown that the dominant contributions to large g values are metal−ligand covalency in the ground and excited states and low-energy charge-transfer excited states. Ligand-based spin−orbit coupling becomes increasingly important as the atomic number of the donor atom increases, but this effect is never the dominant contribution. The series of *cis,trans*-(L-N_2S_2)$Mo^{V}O$(SR) compounds have very similar charge-transfer excited states, as indicated by the similarity of their electronic spectra (Table S33). Also, the ligand-based spin−orbit coupling contributions will essentially be identical because all have three S atoms in the equatorial plane. Therefore, the covalency of the ground and excited states is expected to be similar for the series of *cis,trans*-(L-N_2S_2)-$Mo^{V}O$(SR) compounds.

Table 3 compares the EPR parameters obtained by simulation[37] of the mixed isotope spectra at the S-, X-, and Q-bands of **1** (Figure 5) to those of SO, the "very rapid" signal observed for xanthine oxidase (XO), and other model oxo-Mo(V) systems.[39,40,60] The $A(^{95,97}Mo)$ tensor elements of **1** are distinctly different from those for (tp*)$Mo^{V}O$(bdt) (Table 3), which possesses two S atoms from a benzene dithiolate ligand and whose ground-state involves a unique three-center pseudo-σ type bonding interaction between the Mo d_{xy} orbital and the in-plane S p orbitals of the dithiolate ligand.[45] The EPR parameters of **1** more closely resemble those of the high-pH form of SO and the "very rapid" signal observed for XO than do other oxo-Mo(V) complexes with two or four thiolate ligands (Table 3).

Electrochemistry. The *cis,trans*-(L-N_2S_2)$Mo^{V}O$(SR) complexes undergo a quasi-reversible one-electron reduction and an irreversible oxidation, as revealed by cyclic voltammetry (Table 4). Quasi-reversibility of the reduction couple points

(47) Collison, D.; Mabbs, F. E.; Enemark, J. H.; Cleland, W. E., Jr. *Polyhedron* **1986**, *5*, 423−425.
(48) Collison, D.; Eardley, D. R.; Mabbs, F. E.; Rigby, K.; Enemark, J. H. *Polyhedron* **1989**, *8*, 1833−1834.
(49) Collison, D.; Eardley, D. R.; Mabbs, F. E.; Rigby, K.; Bruck, M. A.; Enemark, J. H.; Wexler, P. A. *J. Chem. Soc., Dalton Trans.* **1994**, 1003−1011.
(50) Garner, C. D.; Lambert, P.; Mabbs, F. E.; King, T. J. *J. Chem. Soc., Dalton Trans.* **1977**, 1191−1198.
(51) Garner, C. D.; Hill, L. H.; Mabbs, F. E.; McFadden, D. L.; McPhail, A. T. *J. Chem. Soc., Dalton Trans.* **1977**, 853−858, 1202−1205.
(52) Nigles, M. J.; Belford, R. L. *J. Magn. Reson.* **1979**, *35*, 259−281.
(53) Balagopalakrishna, C.; Kimbrough, J. T.; Westmoreland, T. D. *Inorg. Chem.* **1996**, *35*, 7758−7768.
(54) Swann, J.; Westmoreland, T. *Inorg. Chem.* **1997**, *36*, 5348−5357 and references therein.
(55) Nipales, N. S.; Westmoreland, T. D. *Inorg. Chem.* **1997**, *36*, 756−757.
(56) Young, C. G.; Enemark, J. H.; Collison, D.; Mabbs, F. E. *Inorg. Chem.* **1987**, *26*, 2925−2927.
(57) Wilson, G. L.; Kony, M.; Tiekink, E. R. T.; Pilbrow, J. R.; Spence, J.; Wedd, A. G. *J. Am. Chem. Soc.* **1988**, *110*, 6923−6925.
(58) Mabbs, F. E.; Collison, D. *Electron Paramagnetic Resonance of d Transition Metal Compounds*; Elsevier Science: Amsterdam, 1992.
(59) Chang, C. S. J.; Collison, D.; Mabbs, F. E.; Enemark, J. H. *Inorg. Chem.* **1990**, *29*, 2261−2267.
(60) Bradbury, J. R.; Mackay, M. F.; Wedd, A. G. *Aust. J. Chem.* **1978**, *31*, 279−284.
(61) Glarum, S. H. *J. Chem. Phys.* **1963**, *39*, 3141−3144.
(62) Garner, C. D.; Hiller, I. H.; Mabbs, F. E.; Taylor, C.; Guest, M. F. *J. Chem. Soc., Dalton Trans.* **1976**, 2258−2261.
(63) Garner, C. D.; Mabbs, F. E. *J. Inorg. Nucl. Chem.* **1979**, *41*, 1125−1127.

toward no or very little structural change during the electrochemical process, while the irreversibility of the Mo^{V}/Mo^{VI} couple could stem from either a gross structural change or facile decomposition of an unstable Mo^{VI} species. Compounds **1** and **2** have more negative reduction potentials than those observed for **3**−**10**. Additionally, the Mo^{V}/Mo^{VI} peak occurs at a lower potential for **1** than for **3**−**10**. Varying the remote substituent (Y) of *cis*,*trans*-(L-N_2S_2)$Mo^{V}O$(*p*-SC_6H_4−Y) results in a significant effect on the observed electrochemical potentials. The reduction potentials and the oxidation peak of the remotely substituted complexes exhibit a linear dependence upon the Hammett parameter, σ_p. The reduction potential varies by 92 mV as the remote substituent is altered from $-OCH_3$ to $-CF_3$, and the oxidation peak changes by 134 mV as the substituent is varied from $-OCH_3$ to $-CF_3$. The linear relationships are expressed in eqs 1 and 2. As expected, the ease of reduction and difficulty of oxidation increase as the remote substituent becomes increasingly electron withdrawing.

$$E_{1/2}\ (\text{reduction}) = 120 \cdot \sigma_p - 946\ (R^2{:}\ 0.988) \qquad (1)$$

$$E_{pa}\ (\text{oxidation}) = 154 \cdot \sigma_p + 420\ (R^2{:}\ 0.965) \qquad (2)$$

Electrochemical oxidation or reduction of the *cis*,*trans*-(L-N_2S_2)$Mo^{V}O$(SR) complexes removes or adds an electron from the HOMO of Figure 4. The sensitivity of the electrochemical potentials of Table 4 to variation of the SR group indicates that the nature of R perturbs the energy of the HOMO. The relative difficulty in the reduction of **1** and **2** compared to **3**−**10** shows that an alkylthiolate ligand destabilizes the HOMO more than the parasubstituted arylthiolates. The reduction and oxidation potentials of the *cis*,*trans*-(L-N_2S_2)$Mo^{V}O$(*p*-SC_6H_4−Y) compounds show that as the electron-releasing ability of the Y substituent on the phenyl ring increases, reduction becomes more difficult and oxidation easier (Table 4). Electron-releasing groups increase the electron density on S2, thereby raising the energy of the HOMO and making reduction more difficult. A similar effect of remote substituents on the reduction and oxidation potentials is exhibited by (tp*)MoO(*p*-OC_6H_4−$Y)_2$, where Y = OMe, OEt, Me, Et, H, F, Cl, Br, I, and CN.[64,65] Likewise, for $CpFe(CO)_2$(*p*-SC_6H_4−Y), where Y = H, Cl, CF_3, and NO_2, the first ionization potential shifts to lower energy as Y becomes less electron withdrawing.[66]

Implications for Molybdoenzymes

The structurally characterized, stable *cis*,*trans*-(L-N_2S_2)$Mo^{V}O$(SR) complexes provide valuable benchmarks for understanding the $Mo^{V}OS_3$ centers of SO and the "very rapid" species of XO, whose electronic structures are extremely difficult to investigate directly. For SO, the electronic absorptions of the Mo center are completely obscured by the intense bands from the *b*-type heme domain for both oxidized[16] and reduced[67] forms of the enzyme. The Mo and heme domains have been cleaved for the rat[68,69] and K108R human[70] sulfite oxidases, but the weak absorptions observed at ∼420, 520, and 550 nm upon sulfite reduction of the Mo domain of rat SO are almost certainly due to minor reduced heme contaminants.[1] Recent MCD difference spectra on the Mo(V) forms of native chicken liver SO show Mo(V) transitions at 22 250, 26 500, and 31 000 cm^{-1}; however, key regions of the spectrum are obscured by the intense temperature-independent *A*- and *B*-terms of the diamagnetic *b*-type Fe(II) heme center.[71] Freeze-quench difference MCD studies of the "very rapid" intermediate of XO show low-energy *C*-terms ascribed to S p to Mo LMCT transitions.[72] Detailed MCD and resonance Raman spectroscopy and theoretical investigations of the *cis*,*trans*-(L-N_2S_2)$Mo^{V}O$(SR) complexes that are in progress should lead to a detailed understanding of the electronic structures of their $Mo^{V}OS_3$ centers. These investigations will also provide a platform for interpreting recent MCD data on the Mo(V) forms of native SO[71] and the "very rapid" species observed for XO.[72]

Acknowledgment. We thank Dr. Arnold Raitsimring and Dr. Frank Mabbs for recording EPR spectra and for many helpful discussions. We acknowledge the Illinois ESR Research Center, NIH Division Research Resources (Grant No. RR01811) for furnishing the EPR Analysis Software. Dr. Jonathan McMaster and Dr. Nadine Gruhn are acknowledged for many helpful discussions, and we thank M. Helton for assistance with the near-IR spectra. A reviewer is thanked for pointing out implications of **1**−**10** for the "very rapid" species of XO. The crystal structures of **1**−**3** were solved as part of an assignment for the crystallography class offered at the University of Arizona. The CCD diffractometer was purchased with funds provided by the National Science Foundation (CHE 9610374). Support of this research by the National Institutes of Health (GM 37773) is gratefully acknowledged.

Supporting Information Available: Tables of EPR data, electronic spectral data for *cis*,*trans*-(L-N_2S_2)$Mo^{V}O$(SR), where R = CH_2CH_3 and *p*-C_6H_4−Y (where Y = CF_3, Cl, Br, F, H, CH_3, CH_2CH_3, and OCH_3), electronic spectra of **3** and **10**, ORTEP diagrams of **2**, **3**, and **10**, and tables of electronic spectral data, crystal data, structure solution and refinement, atomic coordinates, bond length and angles, and anisotropic thermal parameters for **1**−**3** and **10**. This material is available free of charge via the Internet at http://pubs.acs.org.

IC990768O

(64) Graff, J. N.; Basu, P.; Gruhn, N. E.; Chang, J. C.; Enemark, J. H. Manuscript in preparation.
(65) Chang, C. S. J. Ph.D Dissertation, Univerity of Arizona, Tucson, AZ, 1987.
(66) Ashby, M. T.; Enemark, J. H.; Litchenberger, D. L. *Inorg. Chem.* **1988**, *27*, 191−197.
(67) Kipke, C. A.; Cusanovich, M. A.; Tollin, G.; Sunde, R. A.; Enemark, J. H. *Biochemistry* **1988**, *27*, 2918−2926.
(68) Johnson, J. L.; Rajagopalan, K. V. *J. Biol. Chem.* **1977**, *252*, 2017−2025.
(69) Southerland, W. M.; Winge, D. R.; Rajagopalan, K. V. *J. Biol. Chem.* **1978**, *253*, 8747−8752.
(70) Garrett, R. M.; Rajagopalan, K. V. *J. Biol. Chem.* **1996**, *271*, 7387−7391.
(71) Helton, M. E.; Pacheco, A.; McMaster, J.; Enemark, J. H.; Kirk, M. L. *J. Inorg. Biochem.*, submitted for publication, 1999.
(72) Jones, R. M.; Inscore, F. E.; Hille, R.; Kirk, M. L. *Inorg. Chem.* **1999**, *38*, 4963−4970.